View Article Online / Journal Homepage / Table of Contents for this issue

PCCP

Palladium catalysts in the selective hydrogenation of hexa-1,5-diene and hexa-1,3-diene in the liquid phase. Effect of tin and silver addition

Part 1. Preparation and characterization: from the precursor species to the final phases

Emerson Andrade Sales,†[ac] Guy Bugli,[b] Alain Ensuque,[a] Mário de Jesus Mendes[c] and François Bozon-Verduraz*[a]

[a] *Université Denis Diderot (Paris 7), Laboratoire de Chimie des Matériaux Divisés et Catalyse, case 7090. 2, place Jussieu, 75251 Paris Cedex 05, France. E-mail: bozonver@ccr.jussieu.fr*
[b] *Université Pierre et Marie Curie (Paris 6), Laboratoire de Réactivité de Surface et Structure, 4, place Jussieu, 75252 Paris Cedex 05, France*
[c] *Faculdade de Engenharia Química, Unicamp, Caixa Postal 6066, 13083-970, Campinas São Paulo, Brazil*

Published on 01 January 1999. Downloaded on 08/08/2013 20:40:31.

Received 5th November 1998, Accepted 10th December 1998

Palladium, palladium–tin and palladium–silver catalysts, supported on two alumina samples with different acidity, have been prepared by diffusional impregnation for use in the selective hydrogenation of hexa-1,5-diene and hexa-1,3-diene in the liquid phase. UV–VIS–NIR (transmission and diffuse reflectance) studies of the palladium starting solutions and of the solids obtained during all preparation stages (impregnation, drying, calcination) show that the nature of the supported precursor species depends on the acidity of the alumina. Palladium tetrachloropalladate (strongly bound anionic species) are predominant on the more acidic alumina while the more basic one favours the formation of weakly bound neutral complexes through exchange of chloride ligands with hydroxy groups and water. The nature of these species influences not only the particle size of monometallic Pd samples (the stronger the interaction, the smaller the metal particle size), but also the nature of the final bimetallic Pd–Ag catalysts; a Pd–Ag solid solution is observed on the *bimetallic* catalyst prepared by interaction of a cationic Ag precursor *with supported* $PdCl_4^{2-}$, whereas interaction with neutral Pd species leads to separate metal phases. The interaction of Sn precursor solutions with supported Pd^{II} species induces the formation of heteronuclear species which decompose upon drying; Pd_2Sn or Pd_3Sn phases are detected on the final catalysts, depending on the initial Pd/Sn ratio and on the nature of the Sn precursor solvent (using ethanol favours the formation of Pd_3Sn).

1 Introduction

Selective hydrogenations have been used in industry mainly for product value improvement or to eliminate alkadiene and alkyne compounds, sources of operational problems such as plugging due to polymer formation, or contamination of the final product. Whereas cobalt, nickel, molybdenum, chromium and palladium catalysts are reported in the literature for ethyne removal from polyethylene grade ethene,[1–7] only palladium has been employed successfully in industrial operations.

Palladium-based *bimetallic* systems, (with silver, lead or copper as the second metal) were shown to increase the selectivity to ethene, avoiding the addition of carbon monoxide, which promotes the selectivity but is also a contaminant for the subsequent polymerization processes.[3,8,9]

For the selective hydrogenation of alkadienes, palladium catalysts have also proved to be the most active and selective and numerous gas-phase studies have been reported, mostly for buta-1,3-diene hydrogenation;[10–12] the addition of a second metal (Ge, Sn, Pb, Sb, Ag, Ni), leads to contrasting results in the hydrogenation of butadiene or of isoprene;[13–15] whereas the presence of Ni has no beneficial effect,[14] the other metals increase the selectivity to alkenes,[13–15] sometimes with a decrease in activity[15] and the influence of the preparation method was also evidenced.[15] In contrast, very few studies have been conducted in the liquid phase,[16] in spite of some important industrial applications, such as the selective hydrogenation of C_{11}–C_{13} alkadienes present as impurities in alkenes employed in the production of linear alkylbenzenes used as surfactants.

The selective hydrogenation of hexa-1,3-diene and hexa-1,5-diene in the liquid phase may be used as model reactions for the hydrogenation of C_{11}–C_{13} alkadienes; this reaction has already been studied using *monometallic* palladium catalysts[17] but not, to our knowledge, on *bimetallic* systems. A preliminary study of the hydrogenation of hexa-1,5-diene on alumina-supported catalysts, prepared in polyol, showed the influence of silver addition.[18] We now report the effects of tin and silver additives on both the activity and the selectivity of Pd/alumina catalysts prepared by *diffusional* impregnation, *i.e.* where the pore space of the solid is filled with the solvent used for the precursor solution before being contacted with the

† Present address: Instituto de Química Universidade Federal da Bahia Campus Universitário de Ondina, 40170-290 Salvador-Bahia, Brazil.

View Article Online

latter.[19] The selectivity to hex-1-ene is significantly improved in the hexa-1,5-diene hydrogenation but the activity is maintained only for catalysts with a low Sn/Pd ratio.[20a] In order to correlate these performances with the nature of the active phases obtained after the reduction step, special attention has been given to the nature of species involved in the preparation stages.

Here, we present a characterization by UV–VIS–NIR (transmission and diffuse reflectance) spectroscopies of the impregnation solutions and of the solids obtained during all preparation stages. The characteristics of *mono-* and *bimetallic* particles obtained after reduction are studied by transmission electron microscopy (TEM), X-ray line broadening, and H_2 and CO chemisorption; they are tentatively related to the interactions occurring during the preparation steps and to the nature of the precursor species in solution and on the support. Later papers will be devoted to (i) the chemical state and the nature of the active phases, as investigated by Mössbauer Spectroscopy, temperature-programmed reduction (TPR) and IR spectroscopy of adsorbed CO;[20b] and (ii) the catalytic performance in the liquid-phase hydrogenation of hexa-1,3-diene and hexa-1,5-diene.[20a]

2 Experimental

2.1 Materials

Two alumina supports were supplied by Alcoa (support A-1: surface area 63 $m^2\ g^{-1}$, $\alpha + \gamma$ phases; support A-2, surface area 62 $m^2\ g^{-1}$, γ phase only). The zero-point charges, ZPC, determined by the Noh and Schwartz method,[21] are 8.4 and 5.9, respectively. The supports were submitted to diffusional impregnation, *i.e.* they were impregnated first by the solvent and then by a fresh aqueous solution of palladium (II) chloride (Pd concentration: $2.83\text{x}10^{-1}$ mol L^{-1}, pH 2); this solution was prepared by (i) *aqua regia* (HCl/HNO_3 = 3/1) attack of $PdCl_2$; (ii) evaporation to dryness; (iii) dissolution in an HCl aqueous solution. The carrier and the solution were contacted for 16 h; typically, the volume of solution was 3 mL (g of carrier)$^{-1}$; the solvent was then slowly removed by heating at 333 K in vacuum before drying the solid overnight at 383 K. After calcination under synthetic air flow (30 mL min^{-1}) up to 773 K (10 K min^{-1}, plus 3 h at 773 K) two *monometallic* catalysts, labelled as CAT-01 (from support A-1) and CAT-07 (from support A-2) were obtained (Table 1).

Pd–Sn samples were prepared by diffusional impregnation of the non-calcined Pd samples with an aqueous solution of $SnCl_2 \cdot 2H_2O$ (CAT-02 and CAT-04 from CAT-01, CAT-08 from CAT-07) or by an ethanolic solution of the same salt. (CAT-03 from CAT-01). The two Pd–Ag samples (CAT-05 and CAT-09) were prepared by impregnation of non-calcined Pd samples (CAT-01 and CAT-07, respectively) with an aqueous solution of $Ag(NH_3)_2^+$. All these *bimetallic* samples were dried and calcined as described above. In addition, a *monometallic* tin–alumina catalyst (CAT-06) was prepared, by the same procedure, for use as a reference in the Mössbauer experiments (part 2 of this work).[20a] The chemical compositions of the catalysts are listed in Table 1.

2.2 Methods

Chemical analyses were carried out by inductive coupling plasma-atomic emission spectroscopy (ICP–AES) at the Service Central d'Analyse (CNRS-Vernaison). UV–VIS spectra of the solutions were obtained with a Hewlett-Packard 8452A spectrometer. UV–VIS–NIR diffuse reflectance spectrometry (DRS) was performed on a Beckman 5270 spectrometer, equipped with an integration sphere coated with $BaSO_4$, and coupled with an HP microcomputer.

X-ray powder diffraction (XRD) patterns (Cu-Kα radiation) were recorded on a Siemens D500 automatic diffractometer ($10 \leqslant 2\theta/\text{degrees} \leqslant 90$) with a scanning rate of 0.6 degrees min^{-1} [0.02°(2θ) step and 2.0 s counting time]. The diffractometer was calibrated using SiO_2 as a standard. The mean crystallite size was estimated using the Scherrer equation, by computer fitting with Lorentzian and Gaussian lines (software Socabim Diffract-At).

TEM measurements were carried out with a JEOL 100CXII operating at 100 kV. The powder was ultrasonically dispersed in ethanol, and the suspension was deposited on a copper grid coated with a porous carbon film. The particle size distribution was obtained from the TEM pictures using a digital camera and the SAISAM and TAMIS software (Microvision Instruments), calculating the surface-average particle diameter from $d_p = \Sigma n_i d_i^2 / \Sigma n_i d_i$.

X-ray energy dispersive spectrometry (EDX) was performed using a LINK AN 10000 system (Si-Li detector) connected to a JEOL JEM CXII transmission electron microscope operating at 100 kV and equipped with an ASID 4D scanning device (STEM mode). Samples were examined as an ultrafine powder dispersed on copper grids. The X-rays emitted from the specimen upon electron impact were collected in the 0–20 keV range for 200–400 s. Atomic compositions (%) were obtained with the 2LINK program (RTS-2/FLS). The Sn/Pd and Ag/Pd atomic ratios were calculated from the atomic composition, averaged from ten to twelve determinations.

H_2 chemisorption measurements were carried out using a conventional glass volumetric apparatus, following the procedure described by Ragaini and co-workers,[22] avoiding β-PdH formation, but measuring four points. The linear portions of both the total and the reversible chemisorption isotherms were extrapolated to zero pressure to estimate the corresponding uptakes. The fraction of exposed Pd atoms was taken as $(H/Pd)_{irr}$, assuming that the surface stoichiometry of the irreversibly adsorbed hydrogen is unity. The Pd surface area was estimated assuming equal distribution of the (111), (110) and (100) planes, which leads to an atomic area value

Table 1 Elemental analysis of the samples (%) after calcination

Identification	Pd	Sn	Ag	Cl	Cl/Pd atomic ratio
CAT 01 (Pd/A-1)	5.05	—	—	2.31	1.37
CAT 02 (Pd–Sn/A-1)	5.14	3.79	—	2.31	1.35
CAT 03 (Pd–Sn/A-1)	4.89	4.96	—	1.87	1.15
CAT 04 (Pd–Sn/A-1)	5.17	0.77	—	1.56	0.90
CAT 05 (Pd–Ag/A-1)	4.93	—	5.13	[a]	—
CAT 06 (Sn/A-1)	—	4.93	—	1.17	—
CAT 07 (Pd/A-2)	4.55	—	—	3.90	2.57
CAT 08 (Pd–Sn/A-2)	4.12	4.50	—	4.37	3.18
CAT 09 (Pd–Ag/A-2)	3.77	—	5.24	[a]	—

[a] Determination of Cl^- not possible in the presence of Ag. (A-1 and A-2 are alumina samples described in Section 2.1).

Published on 01 January 1999. Downloaded on 08/08/2013 20:40:31.

View Article Online

$A_{Pd} = 7.895 \times 10^{-2}$ nm^2 (Pd atom)$^{-1}$. Considering spherical particles, $d_P = 6\ (V_{Pd}/A_{Pd})/(H/Pd)_{irr}$, where $V_{Pd} = 1.47 \times 10^{-2}$ nm^3 (Pd atom)$^{-1}$ is the atomic volume at 293 K.[23] The substitution of these values gives a simple formula, correlating the dispersion with the mean spherical particle size, expressed in nanometres: $d_P = 1.12/(H/Pd)_{irr}$.

CO chemisorption measurements were also performed on two *monometallic* samples, for comparison. A similar calculation was done with $(CO/Pd)_{irr}$, assuming that the surface stoichiometry of the irreversibly adsorbed CO is unity.[24]

2.3 Reducing pretreatments

All catalysts were reduced, as in TPR experiments,[20a] under flowing H_2 (5% in He) at 30 mL (STP) min^{-1}, by heating from 253 to 773 K, the heating rate being 10 K min^{-1}, with a 10 min stay at the final temperature.

3. Results and discussion

3.1 UV-VIS transmission spectroscopy

The spectrum of the $PdCl_2$ solution (Fig. 1) exhibits (i) one peak near 198 nm, ascribed to charge transfer between chloride ions and water;[25] (ii) four bands attributed to the $PdCl_4^{2-}$ complex ion (D_{4h} symmetry). The two bands at 475 and 336 nm are ascribed to allowed d–d transitions and the other two bands at 279 and 223 nm to ligand–metal charge-transfer (CT) transitions.[26] According to Vogel,[27] dissolution of $PdCl_2$ in *aqua regia* gives $PdCl_4^{2-}$ and $PdCl_6^{2-}$; it follows that evaporation of the solution to dryness leads to the destruction of the latter complex.

The spectra of the aqueous acid (a series) and ethanolic (b series) of $SnCl_2 \cdot 2H_2O$ solutions are presented in Fig. 2. Within each series, the $(i + 1)$th solution is obtained by diluting the ith one with an equal volume of the corresponding solvent. The acid solutions spectra (a series) exhibit an absorption band at *ca.* 214 nm, also observed by Baronetti and coworkers,[28] which may be ascribed to a CT transition between chloride ions and Sn^{IV} ions. This is not unexpected as Sn^{II} *aqueous* solutions always contain Sn^{IV} species[29] resulting from oxidation by air. In an HCl medium, this reaction may be written :

$$SnCl_3^- + 3Cl^- + \tfrac{1}{2}O_2 + 2H^+ \rightleftharpoons SnCl_6^{2-} + H_2O$$

In the acid series, spectrum a1 shows also one band at *ca.* 243 nm, ascribed to a CT transition between chloride and Sn^{II} ions and another near 280 nm, attributed to an intervalence Sn^{II}–Sn^{IV} transition;[30] upon the first dilution (spectrum a2), the latter band is severely decreased (beyond the expected concentration effect) while the second dilution (spectrum a3) removes both bands; this observation is explained by the right shift of the equilibrium written above. The conversion of Sn^{II} species into Sn^{IV} upon dilution explains why the absorbance of the Cl^-–Sn^{IV} CT band does not change significantly.

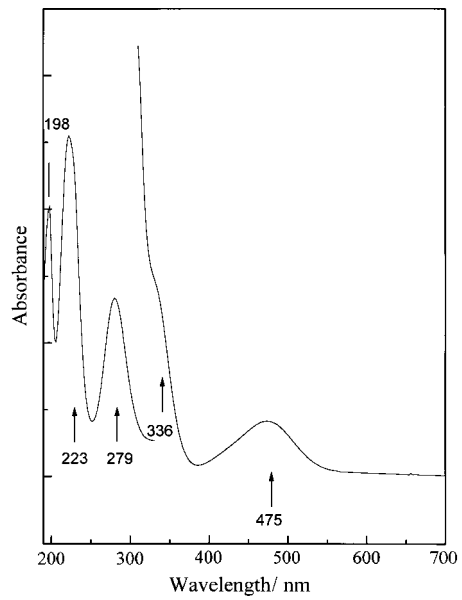

Fig. 1 UV–VIS spectrum of $PdCl_2$ solution (2.8×10^{-3} M) (the right part of the spectrum is expanded 10 times).

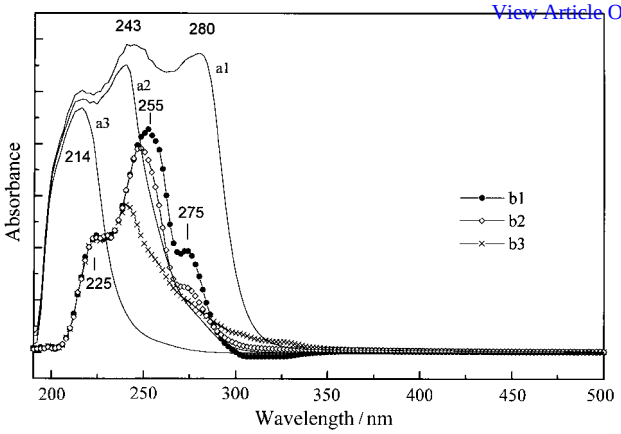

Fig. 2 UV–VIS spectra of $SnCl_2$: (5.3×10^{-3} M): (a) acid solution; (b) ethanolic solution.

The spectra of the ethanolic series b also show three bands, which differ in position and intensity from those of the a series, near 225, 255 and 275 nm. The first band is ascribed to a CT transition between oxygen and Sn^{IV} ions, the significant decrease in absorbance (compared to the a series) giving evidence of the reducing action of ethanol; this band is insensitive to dilution. The band at 255 nm suffers a blue shift upon dilution, unlike the band at 275 nm.

Interaction of $SnCl_2$ solutions with supported Pd^{II}.

When CAT-01 samples were put in contact with the corresponding $SnCl_2$ solution (HCl and ethanol, respectively) to prepare CAT-02 and CAT-03, different colours were developed (brown–green in the former case and red in the latter). In order to discern the role of the solid, the Pd and Sn solutions used for impregnation were mixed, taking a Pd/Sn atomic ratio of 1/1. The orange colour characteristic of the $PdCl_4^{2-}$ solution was kept unchanged using either the hydrochloric or the ethanolic solution of $SnCl_2$. Hence, the brown–green and red colours observed above may arise from reactions involving a *local excess* of Sn^{II} with respect to Pd^{II}, *i.e.* some supported Pd^{II} is dissolved by reaction with the Sn^{II} solution.

To confirm this explanation, Pd and Sn solutions with lower Pd/Sn atomic ratios (*e.g.* 1/5) were mixed; the same brown–green and red colours were observed. We present below a UV-VIS study of this reaction:

(i) Using the *ethanolic* $SnCl_2$ solution, the Pd–Sn solution turns immediately to red; the corresponding UV–VIS spectrum (Fig. 3) exhibits two intense bands near 240 (with a shoulder at 230) and 335 nm, and a weak one near 410 nm. These features may be ascribed to the presence of a heteronuclear Pd–Sn complex. The formation of a Pd^{I}–Sn^{II} complex, indeed, has already been invoked[31] to account for the red colour developed through mixing Pd^{II} and Sn^{II} chloride solutions in an equimolecular mixture of 2M HCl and methanol, with a Pd/Sn atomic ratio of 1 : 5; the same complex could be involved in the present work, as the solvent used (ethanol) is even more reducing than methanol, as indicated by the values of the oxidation potentials,[32] $E^\circ = 0.14$ V for HCO_2H/CH_3OH and $E^\circ = 0.04$ V for CH_3CO_2H/C_2H_5OH.

(ii) With the *aqueous acid* $SnCl_2$ solution, the colour changes from brown to green, passing through dark brown and blue. The reaction was followed by UV–VIS spectroscopy

Published on 01 January 1999. Downloaded on 08/08/2013 20:40:31.

View Article Online

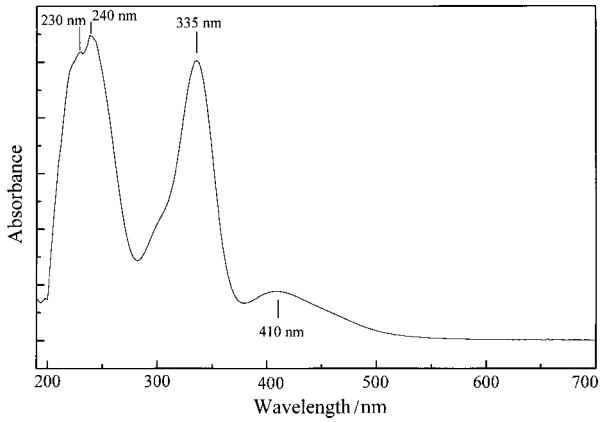

Fig. 3 UV–VIS spectrum of the 1/1 mixture of a $PdCl_2$ solution (2.8×10^{-3} M) and an ethanolic $SnCl_2$ solution (1.4×10^{-2} M).

at 3 min intervals (Fig. 4). The initial spectrum contains one intense band centred near 422 nm and another, weaker and broader, near 584 nm. The final spectrum shows two bands at 464 and 638 nm; it may be ascribed to a complex such as $[PdCl_{4-n}(SnCl_3)_n]^{2-}$, with $2 \leqslant n \leqslant 4$, in agreement with previous results.[33]

Similar data were also obtained by Ayres and Alsop[34] in their spectrophotometric determination of Pd^{II} using Sn^{II} in acid medium, without speculation about the nature of the complex. It is relevant to note that more recent studies on solid clusters generated from Pd^{II}–Sn^{II} hydrochloric solutions[35] claim that inner-sphere redox transformations could even form Pd^{O}-containing species, but this attribution is not supported by the X-ray photoelectron spectroscopy (XPS) data of the authors.

3.2 UV-Visible-NIR DRS spectroscopy

3.2.1 After impregnation and drying (Fig. 5) *Pd/alumina samples (CAT-01) and CAT-07).* The spectra of these samples are different:

(i) on CAT-07, it is clear that $PdCl_4^{2-}$ is the predominant species (bands at 278, 336 and 475 nm, see above), suggesting that this species is formed on the alumina surface during the drying step, as previously reported:[26]

Chloride exchange: $OH^- + H^+Cl^- \rightleftharpoons Cl^- + H_2O$

Deposition of $PdCl_2$: $PdCl_4^{2-} + 2H^+ \rightleftharpoons PdCl_{2\,(s)} + 2H^+Cl^-$

Reaction of $PdCl_2$: $PdCl_2 + 2Cl^- \rightleftharpoons PdCl_4^{2-}$

(ii) on CAT 01, the $PdCl_4^{2-}$ bands are not observed. This is explained by the higher value of the ZPC of the support A-1 (8.4) compared to that of the A-2 carrier (5.9) of CAT 07; this can justify the presence of $PdCl_x(OH)_y(H_2O)_z$ species (with $x + y + z = 4$) on the former sample; OH^- ions or water molecules, indeed, can displace Cl^- ions from the Pd^{II} coordination sphere when the pH increases;[36] this is to be expected when the impregnation solution is contacted with the more basic A-1 support and could lead to the formation of neutral complexes such as $Pd(OH)_2(H_2O)_2$ or $PdCl_2(H_2O)_2$. The formation of such species in solution is well known[36] but the results presented here suggest that such surface precursor species may also appear through contact with alumina.

Pd-Ag samples. CAT 05 and CAT 09 were obtained by diammine silver (I) impregnation; after drying, they show (i) a band near 390 nm, ascribed to unresolved $(\nu_1 + \nu_2)$d–d transitions of $Pd(NH_3)_xCl_y$; this band, indeed, is located between those reported for the D_{4h} complexes $Pd(NH_3)_4^{2+}$ ($\lambda = 297$ nm, $\nu = 33\,700$ cm^{-1}) and $PdCl_4^{2-}$ ($\lambda = 475$ nm, $\nu = 21\,100$ cm^{-1}), respectively;[37] (ii) a weak band near 300 nm ascribed to $Pd(NH_3)_4^{2+}$; (iii) the 2ν harmonics and $(\nu + \delta)$ combination bands of the vibrational spectrum of ammonia (not shown) detected in the NIR at 1549 nm (6460 cm^{-1}) and 2032 nm (4920 cm^{-1}), on both catalysts.

Pd–Sn samples. CAT-02, CAT-03, CAT-04 and CAT-08 exhibit spectra similar to CAT-07, which suggests that $PdCl_4^{2-}$ is the predominant surface species; since contacting the Sn solutions with the Pd^{II} surface species was shown to generate a heteronuclear complex in the solution (see above), it must be concluded that this complex is not predominant on the support or is destroyed during the drying stage.

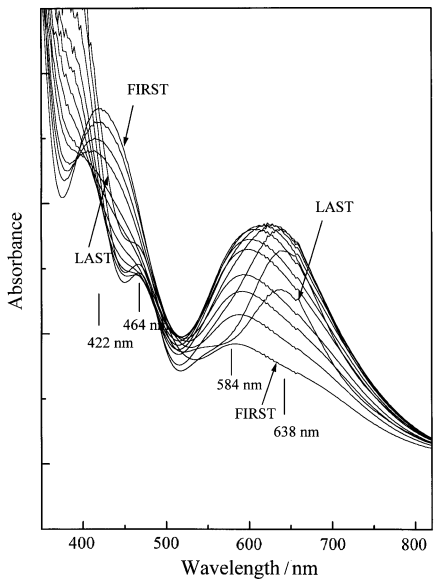

Fig. 4 UV–VIS spectra of the 1/1 mixture of a $PdCl_2$ solution (2.8×10^{-3} M) and an acid $SnCl_2$ solution (1.4×10^{-2} M): evolution with time.

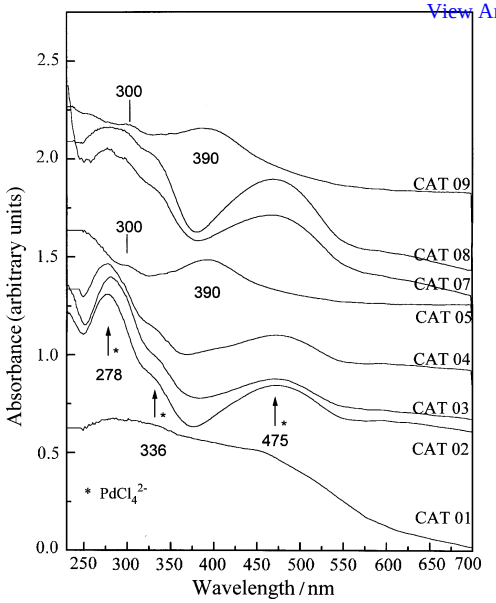

Fig. 5 DRS spectra of impregnated and dried samples

3.2.2. After calcination (Fig. 6). DRS examination shows that $PdCl_4^{2-}$ species are no longer present except for CAT-08 (see below). These spectra display an absorption threshold beginning in the visible region instead of well defined bands.

Published on 01 January 1999. Downloaded on 08/08/2013 20:40:31.

View Article Online

Published on 01 January 1999. Downloaded on 08/08/2013 20:40:31.

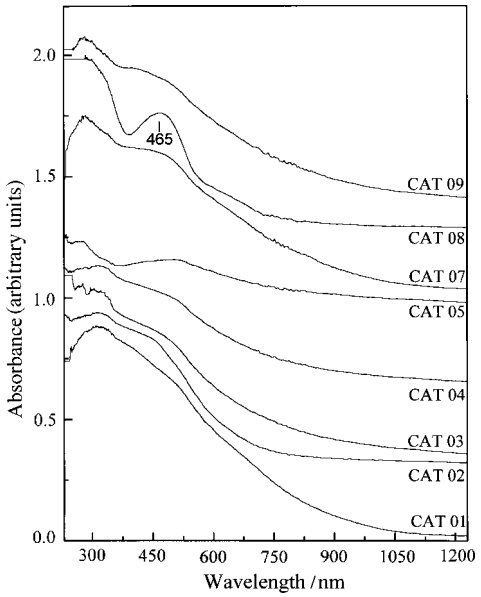

Fig. 6 DRS spectra of calcined samples

In the case of Pd catalysts, this absorption may be attributed to a dispersed Pd^{II} oxide phase;[26a] in fact, bulk PdO is a p-type semiconductor, with a band gap of *ca.* 0.8 eV, giving an absorption threshold at *ca.* 1800 nm, as confirmed by the spectrum of a mechanical mixture PdO/alumina (not shown);[38] however, when the particle size of a semiconductor decreases, the band gap increases, displacing the absorption threshold to lower wavelengths according to the quantum confinement effect.[38] Hence, it may be concluded that the PdO phase is present as small particles on CAT-01 and CAT-07, in agreement with XRD results (see below).

The bimetallic Pd–Sn samples CAT-02, CAT-03 and CAT-04, as well as the Pd–Ag samples CAT-05 and CAT-09, show spectra similar to Pd samples, which suggest that small PdO particles are also present, in agreement with XRD measurements (Section 3.3). On the other hand, catalyst CAT 08 (Pd–Sn) presents a band at 465 nm, which is attributed to a palladium complex with chlorine ligands,[26a] because this catalyst exhibits a high chlorine content (Table 1).

With respect to the Sn/Al_2O_3 catalyst (CAT 06), the spectrum obtained after calcination was compared to that of a mechanical mixture of SnO_2 and alumina (not shown); in both cases, the absorption threshold is located at *ca.* 345 nm (3.6 eV), very close to the value deduced from bulk SnO_2 band gap.[39].

Concerning Pd–Ag samples, CAT-05 shows a flat spectrum compared to CAT-09; it may be related to the contribution of specular reflectance arising from the larger particle size of PdO in the former case.

3.3 XRD

The XRD measurements were carried out on the calcined and on the reduced samples. Besides, the supports, A-1 and A-2 were analysed; both α and γ-Al_2O_3 phases are detected in the former while only the γ-Al_2O_3 phase was present in the latter.

3.3.1 Calcined samples (diagrams not shown). The Pd^{II} oxide phase was identified in all the Pd-containing catalysts. The Ag_2O oxide phase was detected in both Pd–Ag catalysts (CAT-05 and CAT-09) with a large amount of the PdO phase on catalyst CAT-05 and a small amount on the other (CAT-09). Moreover, small peaks of metallic Ag are observed on both catalysts, which is not unexpected because bulk Ag_2O decomposes in air above 160 °C. Finally, on the Sn-containing catalysts, tin was detected only as dioxide (cassiterite).

3.3.2 Reduced samples (Fig. 7 and 8). The XRD patterns show the presence of metallic Pd in all Pd-containing catalysts, except in CAT-02 and CAT-08 where the alloy phase Pd_2Sn is identified (Fig. 7). This Pd_2Sn alloy is not detected on catalyst CAT03, prepared on the same support as CAT-02, but *via* ethanolic impregnation of tin. On the other hand, a Pd_3Sn alloy is identified on this catalyst as well as on CAT-04 (Pd–Sn prepared by an acid route, but with Pd/Sn = 5); these results are confirmed by Mössbauer spectroscopy measurements.[20a]

The XRD patterns of Pd–Ag catalysts, together with their corresponding supports, are shown in Fig. 8 and 9. On cata-

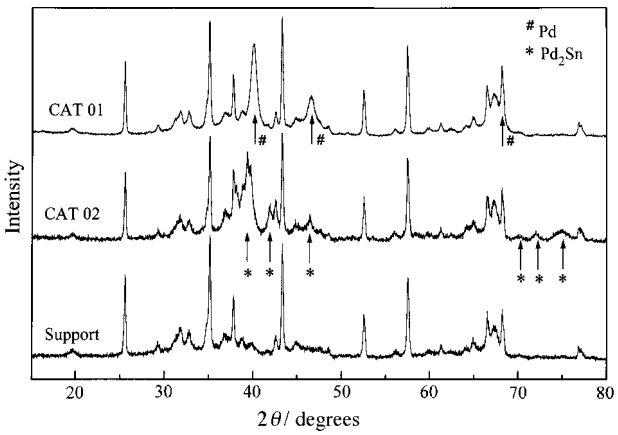

Fig. 7 XRD patterns of reduced catalysts CAT 01 and CAT 02, and of their support (A-1).

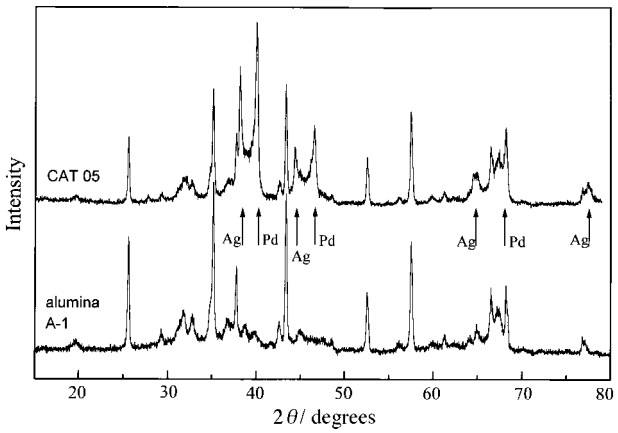

Fig. 8 XRD patterns of reduced Pd–Ag catalyst CAT 05 and of its support (A-1).

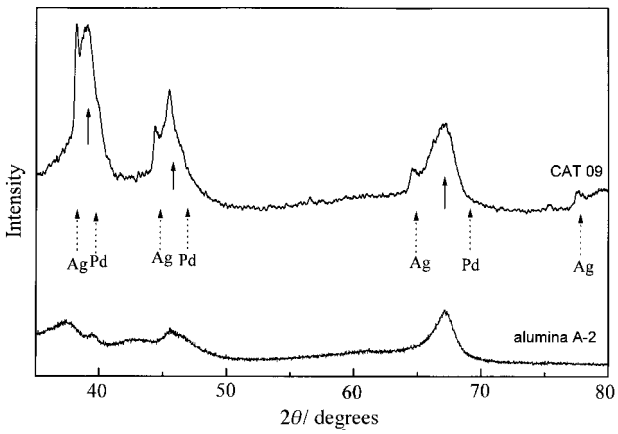

Fig. 9 XRD patterns of reduced Pd–Ag catalyst CAT 09 and of its support (A-2).

View Article Online

Table 2 Reduced samples: identification of phases and comparison of the particle size obtained by various methods

Catalyst	Identified phases	d_p/nm			$(H/Pd)_{irr}$
		XRD	TEM	H_2 chemisorption	
CAT 01	Pd	10	10.8	11.9	0.094
CAT 02	Pd_2Sn	6	8.0	—	0.057
CAT 03 (ethanol)	Pd_3Sn or Pd	6.1	11.0	—	0.061
CAT 04	Pd_3Sn or Pd	2.5	2.2	—	0.28
CAT 05	Ag	35			
	Pd	29	17.4		0.052
CAT 06	SnO_2	100	—	—	
CAT 07	Pd	6.1	5.0	7.4	0.15
CAT 08	Pd_2Sn	7.0	5.5		0.075
CAT 09	Pd–Ag solid solution	4.8	18.0	—	0.033
	Ag	16			

Published on 01 January 1999. Downloaded on 08/08/2013 20:40:31.

lyst CAT-05 (Fig. 8) separate Ag and Pd metallic phases are clearly identified, although a small quantity of Pd–Ag alloy may be present, whereas on CAT-09 a Pd–Ag solid solution is detected, together with some unalloyed Ag (Fig. 9). According to thermodynamic data, Pd–Ag solid solutions are obtained whatever the Pd/Ag ratio;[40] the difference between the two samples, which is at first surprising, may be explained by the nature of the complexes formed upon impregnation: (i) the support A-1 exhibits a higher ZPC (8.4); it was used to prepare the Pd catalyst CAT 01 which contains mainly neutral $Pd(OH)_2(H_2O)_2$ or $PdCl_2(H_2O)_2$ species after impregnation. On the other hand, $PdCl_4^{2-}$ species are detected on the Pd catalyst CAT 07, prepared with the more acidic support A-2. Impregnation by the complex ion $[Ag(NH_3)_2]^+$ should give a stronger interaction with the latter (anionic) species, inducing the formation of a Pd–Ag solid solution on CAT 09 after the activation treatment; on the other hand, the weak interaction of the Ag complex with the neutral complex fixed on A-1 favours the formation of the separate Pd and Ag phases detected on CAT 05.

Table 2 summarizes the identified phases, collects the crystallite sizes estimated by the Scherrer equation and allows comparison with the data from other techniques. It is relevant to note that only SnO_2 is identified on catalyst CAT 06, showing that this phase was not significantly reduced in the absence of palladium, even at 773 K.

3.4 H_2 and CO chemisorption

H_2 chemisorption experiments were performed on all Pd-containing catalysts. Fig. 10 presents the reversibly and irreversibly adsorbed H_2 volumes for CAT 01, CAT 02 and CAT 05. Table 2 collects the values of $(H/Pd)_{irr}$ for all catalysts. The mean metal particle size for Pd catalysts, estimated as cited in Section 2.2, is also presented.

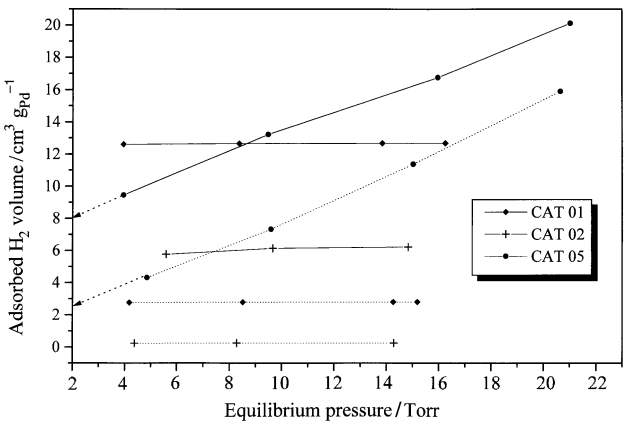

Fig. 10 Total (——) and reversible (– – –) adsorbed H_2 volumes for catalysts CAT 01, CAT 02 and CAT 05.

For bimetallic catalysts CAT-02 and CAT-03, the H/Pd ratio is smaller than for the corresponding Pd catalyst (CAT-01) although their metal particle size is not larger, hence tin atoms may cover a part of the surface Pd atoms or decrease their adsorption capacity;[41] on the contrary, when the Sn/Pd ratio is low (CAT-04), the H/Pd ratio is significantly higher and the metal particle size much smaller; addition of tin at low content is then beneficial for Pd dispersion. On the other hand, in the case of silver-containing catalysts, CAT 05 (Fig. 10) and CAT 09 (not shown) neither total nor reversible isotherms show a plateau, in agreement with previous results on unsupported Pd–Ag alloys.[42] This phenomenon may be explained by promotion of hydrogen absorption due to the formation of Pd–Ag alloys. The H/Pd values, presented in Table 2, for these catalysts are obtained from the difference between the total and reversible adsorbed H_2 volumes, that remain almost constant, extrapolated to zero pressure.

Using the same procedure, CO chemisorption experiments were performed on the monometallic catalysts, assuming that the surface stoichiometry of the irreversibly adsorbed CO is unity.[24] The corresponding values of the particle size (Table 3) are *ca.* 15% higher than with hydrogen; this overestimation

Table 3 Reduced catalysts: CO adsorbed volumes [cm^3 (g Pd)$^{-1}$], $(CO/Pd)_{irr}$ and mean particle size (d_p)

Catalyst	V_{REV}^{CO}	V_{IRR}^{CO}	$(CO/Pd)_{irr}$	d_p/nm
CAT 01	4.44	15.94	0.076	14.7
CAT 07	4.26	28.39	0.135	8.3

Table 4 Atomic Sn/Pd and Ag/Pd ratios for the bimetallic catalysts, averaged from STEM–EDX analysis, and comparison with the bulk chemical composition from ICP–AES

		CAT 02	CAT 03	CAT 04	CAT 08
Sn/Pd	STEM–EDX	0.50	0.41	0.11	0.61
	ICP–AES	0.66	0.91	0.13	0.98
		CAT 05	CAT 09		
Ag/Pd	STEM–EDX	1.10	1.67		
	ICP–AES	1.03	1.37		

View Article Online

may arise from an underestimation of the volume of adsorbed CO, because a part of the less weakly bound linear CO species is reversibly chemisorbed, as evidenced by IR spectroscopy.[24]

3.5 TEM and STEM-EDX

3.5.1 Pd/Al_2O_3 catalysts. The catalyst CAT 01 shows a larger mean particle size (10.8 nm) than CAT 07 (5 nm, with a particle size distribution from 1.0 to 7.5 nm, TEM micrographs not shown), which is not very different from the values obtained from XRD measurements (Table 2). Hence it may be concluded that the particles observed by TEM are single crystals. The smaller particle size obtained on CAT-07 is ascribed to the stronger precursor–carrier interaction due to the acidic character of the carrier A-2 of CAT-07 (see above, Section 3.2).

3.5.2 $Pd–Sn/Al_2O_3$ catalysts. TEM examination of the catalysts CAT-02 (Pd–Sn/A-1, acid route) and CAT 03 (Pd–Sn/A-1, ethanolic route) shows small particles and aggregates; hence, an average diameter value is not convenient to represent the actual morphology of these samples; in contrast, catalysts CAT-04 (Pd–Sn/A-1, Sn/Pd ≠ 1/8) and CAT-08 (Pd–Sn/A-2, Sn/Pd ≠ 1) exhibit only small ($d_P \sim 2.2$ and 5.5 nm, respectively) and rather uniformly distributed metal particles; the agreement with XRD data still suggests that these particles are single crystals. These results may be related to the stronger precursor–carrier interaction in the case of CAT-08, but no immediate explanation is available for CAT-04.

Moreover, STEM-EDX results (Table 4) indicate systematically lower Sn/Pd atomic ratios than the bulk chemical composition; this is apparently in contradiction to the Sn enrichment of the outer layers expected from thermodynamics.[41–43] However, other Sn-rich phases are present; SnO_2 and $SnAl_2O_5$ have been evidenced by Mössbauer spectroscopy[26a] and the former is also detected by DRX (see above); this may account for this apparent Pd segregation.

3.5.3 $Pd-Ag/Al_2O_3$ catalysts. According to STEM-EDX experiments, CAT 05 shows both Pd-rich (up to 70%) and Ag-rich (up to 90%) particles and the Ag/Pd ratio presented in Table 4 represents only an average value; this is in agreement with the XRD patterns of this sample, which show Pd and Ag metallic phases. In contrast, the composition of CAT-09 is much more uniform; this is in accordance with the presence of a Pd–Ag solid solution, even though some unalloyed Ag is detected; moreover, as the Ag concentration is higher than the bulk composition (Table 4), an Ag enrichment of the outer layer occurs in the solid solution, which is consistent with the lower sublimation heat of this element.[41,44]

3.6 Comparison of the particle size and dispersion measurements

Table 2 summarizes the results of the particle size determinations by different techniques (chemisorption for monometallics, TEM and XRD). For the monometallic catalysts, it appears that the particles observed by TEM are single crystals. For bimetallic samples, the particle size deduced from XRD is only an estimate as compositional non-uniformity may contribute to peak broadening; in some cases (CAT-03, CAT-09), TEM observations give significantly larger sizes than XRD; this means that the particles observed by TEM are aggregates of single crystals of *ca.* 5–6 nm. In contrast, for the Pd–Sn catalyst with low Sn loading (CAT 04), it is concluded that the particles observed by TEM are elemental crystals; in the case of the Pd–Ag sample CAT-05, XRD and TEM data show the heterogeneity of the sample.

4 Conclusions

The nature of Pd^{II} species fixed on the alumina carrier by diffusional impregnation depends on the acidity of alumina, because precursor interactions may occur not only at the solid/liquid interface but also upon drying; $PdCl_4^{2-}$ species are predominant on the most acidic alumina while weakly bound species, such as $PdCl_2(OH)_2(H_2O)_2$ and $Pd(OH)_2(H_2O)_2$ are formed on the more basic one. The nature of these species influences not only the particle size of monometallic Pd samples (the stronger the interaction, the smaller the metal particle size), but also the nature of the final bimetallic Pd–Ag catalysts; a Pd–Ag solid solution is observed on the bimetallic catalyst prepared by interaction of a cationic Ag precursor with supported $PdCl_4^{2-}$, while interaction with neutral Pd species leads to the predominance of separate metal phases.

The interaction of Sn precursor solutions with supported Pd^{II} species induces the formation of heteronuclear species, which are not observed on the carrier after drying; Pd_2Sn or Pd_3Sn phases are detected on the final catalysts, depending on the Pd/Sn initial ratio and on the nature of the Sn precursor solvent (the use of ethanol favours the formation of Pd_3Sn). The formation of Pd–Sn compounds or alloys from the heteronuclear species deserves further examination. Additional information based on an IR study of CO chemisorption, XPS examination, TPR studies and Mössbauer measurements will be given in Part 2 of this work.[20b]

Acknowledgements

The authors are grateful to P. Beaunier and M. Lavergne for their help in electron microscopy experiments, and to M. H. A da Silva for her help in XRD analysis of calcined samples. We also gratefully acknowledge the CNPq (Brasil) for financial support that allowed this international cooperation.

References

1 R. E. Reitmer and H. W. Feming, *Chem. Eng. Prog.*, 1958, **54**, 48.
2 G. C. Bond and P. B.Wells, *J. Catal.*, 1966, **5**, 419.
3 G. C.Bond, D. A. Dowden and N. Mackenzie, *Trans. Faraday Soc.*, 1958, **54**, 1537.
4 A. J. Den Hartog, M. Deng, F. Jongerius and V. Ponec, *J. Mol. Catal.*, 1990, **60**, 99.
5 A. N. R. Bos, E. S. Bootsma, F. Foeth, H. W. J. Sleyster and K. R. Westerterp, *Chem. Eng. Process.*, 1993, **32**, 53.
6 N. Itoh, W. C. Xu and A. M. Sathe, *Ind. Eng. Chem. Res.*, 1993, **32**, 2614.
7 K. Otsuka and T. Yagi, *J. Catal.*, 1994, **145**, 289.
8 (a) A. H. Weiss, S. Leviness, V. Nair, L. Guczi, A. Sarkany and Z. Schay, in: Proceedings of the 8th International Congress on Catalysis, Verlag Chemie, Berlin, 1984, vol. 5, p. 591; (b) S. Leviness, V. Nair, A. H. Weiss, Z. Schay and L. Guczi, *J. Mol. Catal.*, 1984, **25**, 131.
9 H. R. Adúriz, C. E. Gígola, A. M. Sica, M. A Volpe and R. Touroude, *Catal. Today*, 1992, **15**, 459.
10 G. C. Bond, *Catalysis by Metals*, Academic Press, London, 1962, p. 297.
11 A. Borgna, J. Moraweck, J. Massardier and A. Renouprez, *J. Catal.*, 1991, **128**, 99.
12 (a) J. P. Boitiaux, J. Cosyns and S. Vasudevan, *Appl. Catal.*, 1983, **6**, 41. (b) J. Goetz, M. A. Volpe and R. Touroude, *J. Catal.*, 1996, **164**, 369.
13 (a) P. M. Rylander, *Catalytic Hydrogenation in Organic Syntheses*, Academic Press, New York, 1979; (b) M. Meyer, N. Barbouth and J. Oudar, *C.R. Acad. Sci. Paris*, 1990, **311 (série II)**, 313.
14 A. Renouprez, J. F. Faudon, J. Massardier, J. L. Rousset, P. Delichère and G. Bergeret, *J. Catal.*, 1997, **170**, 181.
15 H. R. Aduriz, P. Bodnariuk, B. Coq and F. Figueras, *J. Catal.*, 1989, **119**, 97.
16 (a) W. G. Young, R. L Meier, J. Vinograd, H. Bollinger, L. Kaplan and S. L. Linden, J. *Am. Chem. Soc.*, 1947, **69**, 2046; (b) C. Fragale, M. Gargano, N. Ravasio, M. Rossi and I. Santo, *J. Mol. Catal.*, 1984, **24**, 211.

Published on 01 January 1999. Downloaded on 08/08/2013 20:40:31.

View Article Online

17 (a) L. Horner and I. Grohmann, *Liebigs Ann. Chem.*, 1963, **670**, 1; (b) K. H. Stadler, M. Schneider and H. Kochloefl, in ref. 8(a), p. 229.
18 E. A. Sales, B. Benhamida, V. Caizergues, J. P. Lagier, F. Fievet and F. Bozon-Verduraz *Appl. Catal. A*, 1998, **172**, 273.
19 M. Che, O. Clause and C. Marcilly, in *Handbook of Heterogeneous Catalysis*, ed. G. Ertl, H. Knözinger and J. Weitkamp, VCH, Weinheim, 1997. vol. 1, p. 191.
20 (a) E. A. Sales, M. J. Mendes and F. Bozon-Verduraz, in preparation; (b) E. A. Sales, J. Jove, M. J. Mendes and F. Bozon-Verduraz, in preparation.
21 J. S. Noh and J. A. Schwarz, *J. Colloid Interface Sci.*, 1989, **30**, 157.
22 V. Ragaini, R. Giannantonio, P. Magni, L. Lucarelli and G. Leofanti, *J. Catal.* 1994, **146**, 116.
23 S. Ichikawa, H. Poppa and M. Boudart, *J. Catal.*, 1985, **91**, 1.
24 D. Tessier, A. Rakai and F. Bozon-Verduraz, *J. Chem. Soc. Faraday Trans.*, 1992, **88**, 741.
25 L. I. Katzin, *J. Chem. Phys.*, 1955, **23**, 2055.
26 (a) A. Rakai, D. Tessier and F. Bozon-Verduraz, *New J. Chem.*, 1992, **16**, 869; (b) F. Bozon-Verduraz, A. Omar, J. Escard and B. Pontvianne, *J. Catal.*, 1978, **53**, 126.
27 A. I. Vogel, *Textbook of Macro and Semimicro Qualitative Inorganic Analysis*, Longman, London, 5th edn., 1979.
28 G. T. Baronetti, S. R. Miguel, O. A. Scelza, M. A. Fritzler and A. A. Castro, *Appl. Catal.*, 1985, **19**, 77.
29 F. A. Cotton and G. Wilkinson, *Advanced Inorganic Chemistry*, Interscience, New York, 1972, p. 331.
30 G. C. Allen and N. S. Hush, *Prog. Inorg. Chem.*, 1967, **8**, 357.
31 M. A. Khattak and R. J. Magee, *J. Chem. Soc. Chem. Commun.*, 1965, **17**, 400.
32 W. M. Latimer, *The Oxidation States of the Elements and Their Potentials in Aqueous Solutions*, Prentice-Hall, New York, 2nd edn., 1952, p. 400.
33 (a) V. I. Shlenskaya, A. A. Biryukov and L. N. Mooryakova, *Russ. J. Inorg. Chem.*, 1969, **14**, 255; (b) S. Manolov, K. Davarski and N. Khalachev, *Russ. J. Inorg. Chem.*, 1991, **36**, 1355 ; (c) A. I. Zayats, T. S. Psareva and V. F. Shabanov, *Russ. J. Inorg. Chem., 1976*, **21**, 393.
34 G. H. Ayres and J. H. Alsop, *Anal. Chem.*, 1959, **31**, 1135.
35 E. N. Yurchenko and G. L. Elizarova, *Russ. J. Inorg. Chem.*, 1987, **32,** 1595.
36 (a) C. F. Baes and R. E. Messmer, *The Hydrolysis of Cations*, Wiley, New York, 1976; (b) L. I. Elding and L. F. Olsson, *J. Phys. Chem.*, 1978, **82**, 69.
37 M. Che and F. Bozon-Verduraz, in ref. 19, vol. 2, p. 641.
38 A.Rakaï, A. Bensalem, J. C. Muller, D. Tessier and F. Bozon-Verduraz, *Stud. Surf. Sci. Catal.*, 1993, **75B**, 875.
39 N. Tsuda, K. Nasu, A. Yanase and K. Siratori, *Electronic Conduction in Oxides*, Springer Verlag, Berlin, 1983, p. 116.
40 I. Karakaya and W. T. Thompson, *Bull. Alloy Phase Diagrams*, 1988, **9**, 237.
41 V. Ponec and G. C. Bond, *Stud. Surf. Sci. Catal.*, 1995, **95**, 393
42 E. G. Allison and G. C. Bond,. *Catal. Rev.*, 1972, **7**, 233.
43 R. P. Elliott, *Constitution of Binary Alloys*, Genium Publishing, New York, 1st Supplement, 1985, p. 733.
44 A. El Hamdaoui, G. Bergeret, J. Massardier, M. Primet and A. Renouprez, *J. Catal*, 1994, **148**, 47.

Paper 8/08666D

Published on 01 January 1999. Downloaded on 08/08/2013 20:40:31.